Chain End Mobilities in Polymer Melts – A Computational Study

Diddo Diddens[1, 2, *] and Andreas Heuer[1, 2]

[1] *Institut für physikalische Chemie, Westfälische Wilhelms-Universität Münster, Corrensstrasse 28/30, 48149 Münster, Germany*

[2] *NRW Graduate School of Chemistry, Corrensstrasse 36, 48149 Münster, Germany*

(Dated: August 16, 2012)

The Rouse model can be regarded as the standard model to describe the dynamics of a short polymer chain under melt conditions. In this contribution, we explicitly check one of the fundamental assumptions of this model, namely that of a uniform friction coefficient for all monomers, on the basis of MD simulation data of a PEO melt. This question immediately arises from the fact that in a real polymer melt the terminal monomers have on average more intermolecular neighbors than the central monomers, and one would expect that exactly these details affect the precise value of the friction coefficient according to the Fluctuation-Dissipation Theorem. The mobilities are determined by our recently developed statistical method[1], which provides complementary information about the local polymer dynamics and thus contrasts standard quantities such as the mean square displacement (MSD) or the Rouse mode analysis. Within our analysis it turned out that the Rouse assumption of a uniform mobility is fulfilled to a good approximation for the PEO melt, although the underlying microscopic dynamics is highly affected by different contributions from intra- and intermolecular excluded volume interactions, which, each in itself, cannot be taken into account by a modified friction coefficient. However, in the sum, these non-trivial terms roughly cancel each other, and the overall dynamics corresponds to that of a phantom chain. These effects remain elusive when studying the dynamics with the MSD only, since this observable characterizes a sum over dynamical contributions due to the bare mobility, chain connectivity and more complicated local potentials.

PACS numbers: 36.20.Ey 61.25.H-

I. INTRODUCTION

The Rouse model[2,3] is one of the standard models to describe the dynamics in a polymer melt of non-entangled chains. Here, the polymer chain is modeled as a sequence of N harmonically linked beads. All intermolecular interactions of the chain are reduced to a frictional and a stochastic force, both characterized by the friction coefficient ζ via the Fluctuation-Dissipation Theorem[3]. Within this model, ζ takes the same value for all beads irrespective of the monomer position n. However, when going to real polymer melts, it is obvious that the individual polymer segments along the chain cannot have exactly the same intermolecular environment due to chain connectivity. A terminal segment has on average more intermolecular neighbor segments in its first coordination sphere than a segment located in the center of the chain. Therefore, it is questionable if the assumption of a uniform friction constant along the entire chain as assumed in the Rouse model still holds for a realistic chain in the melt.

The dynamics of the chain ends also plays a special role in the limit of long chains, which is usually described by the reptation model[4]. Within this picture, the topological constraints imposed by the other chains are modeled as a tube[3], and the tagged chain performs Rouse-like motion within this effective tube. Here, the local dynamics of the chain ends play an important role in a twofold manner: First, since the chain can only escape the tube at its ends, one would expect that the dynamics of the chain ends significantly influences the overall relaxation mechanism. For example, it has been observed in simulations[5–7] that the tube constraints are less pronounced for the terminal monomers. Improved models suggest that the tube relaxation is enhanced by so-called contour-length fluctuations[3], which have also been observed experimentally[8]. Here, the motion of the chain ends leads to a loss of memory of the initial tube. Second, switching to the surrounding chains imposing the tube constraint, it was argued that the chain ends do not contribute to the formation of entanglements, and a revised tube model has been proposed[9,10]. Experimental data of a bimodal melt was successfully interpreted within this concept[11].

A different but related interplay of topological constraints and the chain end dynamics becomes important if a polymer melt approaches the glass transition temperature T_g. The dependence of T_g on the molecular weight is usually described by the empirical Flory-Fox equation[12]. Within this picture, the chain ends experience a larger amount of free volume than the central monomers, leading to a lower T_g for short chains, which has also been observed in MD simulations[13].

For all these reasons, the specific role of the chain-end dynamics as compared to the motion of the central parts of the chain is a long-standing issue in polymer science, which has naturally already been investigated by several experimental[14–17] and numerical[5–7,18] studies. However, when discussing 'segmental mobilities', one should keep in mind that this expression may refer to essentially two different microscopic quantities: On one hand, the segmental mobility may be equal to the inverse Rouse friction coefficient, ζ^{-1}, which is determined by the inter-

molecular collisions on short time scales according to the Fluctuation-Dissipation Theorem[3]. On the other hand, the same term is used to describe how fast a given segment moves, and thus rather corresponds to a superposition of chain-connectivity effects (which are naturally less pronounced for terminal monomers) and the bare Rouse mobility ζ^{-1}. Within this context, one should also keep in mind that most experiments such as spin-labeling techniques[14,16,17] or neutron reflectivity[15]/neutron spin echo[8,11] measurements as well as the standard observables calculated from simulation data such as the mean square displacement (MSD)[5–7,18] quantify the net movement of a polymer segment, and thus rather characterize the complex interplay between chain connectivity, bare mobility and more complicated many-chain effects.

In contrast to this, we focus on the first definition given above, namely the bare Rouse mobility ζ^{-1}. In particular, we check the classical Rouse assumption of a uniform ζ-value for all polymer segments independent of their position within the chain (i. e. at the end or in the center) for the case of a realistic PEO chain under melt conditions. This is a highly pertinent question, since it is obvious that the intermolecular environment, which determines the precise value of ζ within the picture of Brownian motion[3], is significantly different for a terminal and a central PEO monomer. In order to address this issue, we apply our recently developed method to determine segmental mobilities (pq-method[1]) to atomistic MD simulations of a PEO melt. It has been devised to extract this specific informaton about the *local* friction. The results from the MD simulations are interpreted within the simpler semiflexible chain model (SFCM[19]), in which a Rouse chain is augmented by an additional angle potential, thus incorporating chain stiffness. From a technical point of view, additional emphasis is put on the comparison of our method with conventional dynamical quantities such as the MSD. In the course of our analysis, interesting chain end effects are observed, which cannot be captured by a modified friction coefficient, but rather reflect more subtle intra- and interchain interactions.

II. SIMULATION DETAILS

For our analysis, MD simulation data of a PEO melt from a previous study[20] has been used. The system consisted of 16 PEO chains with $N = 48$ monomers each. The simulations were performed in the NVT ensemble with the GROMACS simulation package[21] using an effective two-body polarizable force field[22]. The temperature had been maintained at $T = 450$ K by a Nosé-Hoover thermostat.

Additionally, the SFCM[19] has been simulated via Brownian Dynamics (BD) Simulations. In this model, a Rouse chain is augmented by a bending potential

$$U_\theta(\{\mathbf{R}_n\}) = -k_\theta \sum_{n=2}^{N-1} \frac{(\mathbf{R}_{n+1}-\mathbf{R}_n)(\mathbf{R}_n-\mathbf{R}_{n-1})}{|\mathbf{R}_{n+1}-\mathbf{R}_n||\mathbf{R}_n-\mathbf{R}_{n-1}|}\,, \quad (1)$$

where the $\mathbf{R}_n$ correspond to the position vectors of the beads. Here, the value of $k_\theta/(k_\mathrm{B}T) = 2.1$ has been chosen, for which we found that the characteristic ratio of the SFCM matches that of the PEO chains in the MD simulations. Naturally, the semiflexible chains contained the same number of monomers ($N = 48$) as the PEO chains. For the friction coefficient ζ, the temperature $k_\mathrm{B}T$ and the mean squared bond length b^2, unit values were used. In this case, a time-step of $\Delta t = 0.002$ turned out to be sufficiently small in order to propagate the system with a simple Euler integrator.

III. PQ-METHOD

To briefly review the pq-method[1], we start with a stroboscopic view on the local Langevin dynamics of monomer n of a polymer chain

$$\mathbf{p}_n(t,\Delta t) = -A_n(\Delta t)\mathbf{q}_n(t) + \text{noise}\,, \quad (2)$$

where the definitions

$$\mathbf{p}_n(t,\Delta t) = (1/\Delta t)\,[\mathbf{R}_n(t+\Delta t) - \mathbf{R}_n(t)] \quad (3)$$

and

$$\mathbf{q}_n(t) = 2\mathbf{R}_n(t) - \mathbf{R}_{n+\Delta n}(t) - \mathbf{R}_{n-\Delta n}(t) \quad (4)$$

have been used. In case of the terminal monomers, eq. 4 can be modified according to $\mathbf{q}_1 = \mathbf{R}_1 - \mathbf{R}_{1+\Delta n}$ and $\mathbf{q}_N = \mathbf{R}_N - \mathbf{R}_{N-\Delta n}$ (fig. 1). For polymer chains with a certain stiffness, Δn corresponds to the number of chemical monomers within one Kuhn segment, and was chosen such that $C_\infty \approx [\langle(\mathbf{R}_n-\mathbf{R}_{n-\Delta n})^2\rangle/\langle(\mathbf{R}_n-\mathbf{R}_{n-1})^2\rangle]^{1/2}$ is approximately fulfilled. The characteristic ratio in turn was determined from the mean squared end-to-end vector $\langle\mathbf{R}_\mathrm{e}^2\rangle$ using the identity $C_\infty = \langle\mathbf{R}_\mathrm{e}^2\rangle/[(N_0-1)b_0^2]$, where b_0^2 is the average squared distance between two chemical monomers (in total N_0). For PEO ($C_\infty = 3.2$), $\Delta n = 4$ was obtained. Due to the choice of k_θ in eq. 1, the same Δn-value was used for the SFCM.

Eq. 2 serves as a definition of a time-dependent, effective mobility $A_n(\Delta t)$, which for a Rouse chain with $\Delta n = 1$ approaches the true ratio k/ζ in the limit $\Delta t \to 0$. Here, $k = 3k_\mathrm{B}T/b^2$ is the entropic force constant and b^2 the average squared bond length between two Kuhn segments. For finite Δt and appropriate Δn eq. 2 maps the local dynamics of a more realistic chain (i. e. the SFCM or PEO) onto the Langevin dynamics of a Rouse bead, thus yielding an effective mobility $A_n(\Delta t)$ for bead n on the time scale Δt. From simulation data, $A_n(\Delta t)$ can easily be determined by a linear regression

$$A_n(\Delta t) = \frac{\langle p_{n,\alpha}(\Delta t) q_{n,\alpha}\rangle}{\langle q_{n,\alpha}^2\rangle} = \frac{\langle \mathbf{p}_n(\Delta t)\mathbf{q}_n\rangle}{\langle \mathbf{q}_n^2\rangle}\,, \quad (5)$$

where α represents the Cartesian coordinates and $\langle p_{n,\alpha}(\Delta t)\rangle = \langle q_{n,\alpha}\rangle = 0$ due to isotropy.

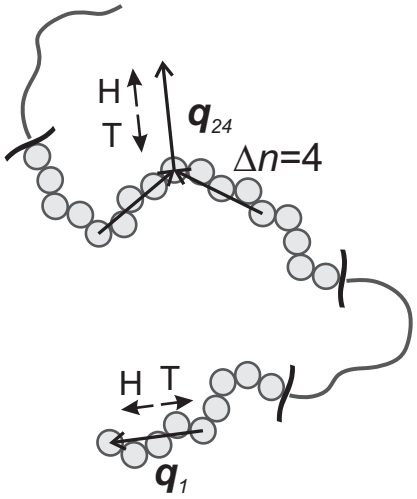

Figure 1: Sketch depicting various definitions used in the present analysis for a simplified excluded volume chain. Depending on the direction in which the center of mass of the subchain consisting of all monomers within $\mathbf{q}_n$ moves during time Δt, one can distinguish between head (H) and tail (T) monomers (see text for further explanation).

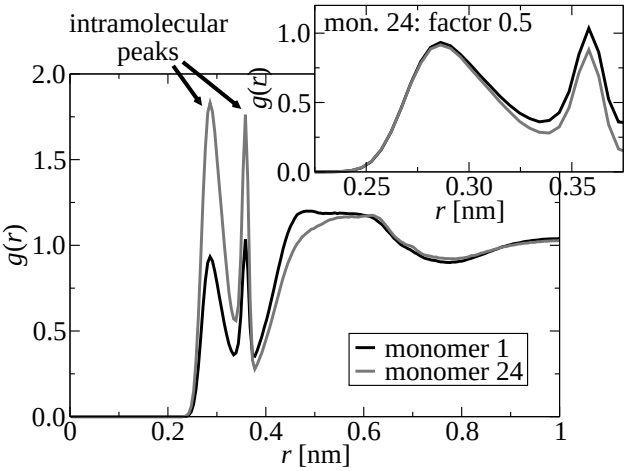

Figure 2: Radial distribution function of the terminal ($n = 1$ and $n = 48$) and the central ($n = 24$ and $n = 25$) PEO monomers in the melt. The average was performed over all chains and all initial time frames. For clarity, the curve of the central monomer has been divided by two in the inset.

Because of the additional backdragging forces, exerted by the remaining part of the polymer chain at longer times, $A_n(\Delta t)$ naturally decreases with increasing Δt. On the other hand, the dynamics in the femtosecond regime is governed by the local chemical structure and by ballistic effects. We found in our previous work[1] on the same simulation data that $A(\Delta t)$, when averaged over all monomers except the five outermost, shows quantitative agreement for the SFCM and PEO from approximately 5 ps. Due to this agreement, we will use the $A_n(\Delta t)$-curves of the individual SFCM monomers to interpret the results for PEO. Moreover, we also observed in ref.[1] that $A(\Delta t)$ for both PEO and the SFCM contains additional anharmonic contributions on time scales shorter than several ten to hundred picoseconds. Thus, for the short-time regime, the microscopic polymer structure manifests itself in the form of additional terms of higher order than the linear relationship given by Eq. 2. In order to remove these rather delicate features, we modified Eq. 2 in the present analysis by additionally taking into account a cubic term, thus allowing us to extract the linear, Rousean contribution separately. Of course, this modification does not affect our method from a conceptual point of view.

IV. STRUCTURAL PROPERTIES

We start with the radial distribution function of the ether oxygens of the PEO chains. This quantity has been computed for both the terminal ($n = 1$ and $n = 48$) and the central ($n = 24$ and $n = 25$) PEO monomers (fig. 2). The average has been performed over all chains in the simulation box as well as over all initial time frames. Up to approximately 0.4 nm, two intramolecular peaks around $r = 0.28$ nm and $r = 0.36$ nm can be observed, corresponding to the neighbor monomer(s). The occurrence of two peaks indicates the existence of two preferred conformations (note that the root mean squared distance between the oxygen atoms of two bonded monomers is about 0.32 nm). Naturally, these peaks are approximately twice as high for $n = 24$ due to chain connectivity (see inset of fig. 2, where the curve of monomer 24 has been divided by two). When going to distances of about $0.4 - 0.5$ nm, one indeed observes that the terminal monomer has more intermolecular neighbors in its first coordination shell than the central monomer.

Of course, these observations are not very surprising, since the different intermolecular *structure* in the vicinity of terminal and central monomers seems only logical. However, as pointed out above, exactly these differences may also alter the *dynamical* behavior beyond the general differences due to the dissimilar chain connectivity, which are already contained in the Rouse model.

V. MEAN SQUARED DISPLACEMENT

In order to get a first impression of the local polymer motion, we start with the MSD, which can be regarded as a standard tool to study the dynamics in simulations.

For the MSD of the entire PEO chains, we naturally observe the well-known subdiffusive center-of-mass motion on time scales shorter than the Rouse time τ_R (not shown), which has been found in several simulations[18,23–26], experiments[25,27] and theoretical analyses[28,29]. It is generally believed that the subdiffusivity for realistic chains is caused by a combination of the excluded volume interactions and chain connectivity, giv-

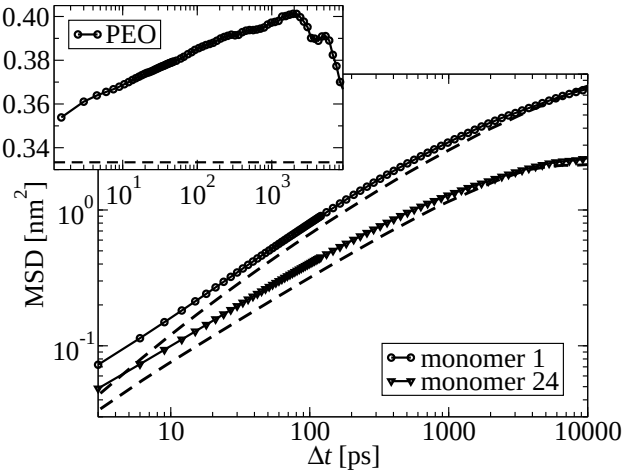

Figure 3: MSD in the center-of-mass frame of the terminal and the central monomers for PEO (symbols) and the SFCM (dashed line). The inset shows the ratio of the center-of-mass MSD in direction of $\mathbf{R}_e$ and the total center-of-mass MSD for PEO. The dashed line indicates the ideal value for isotropic diffusion.

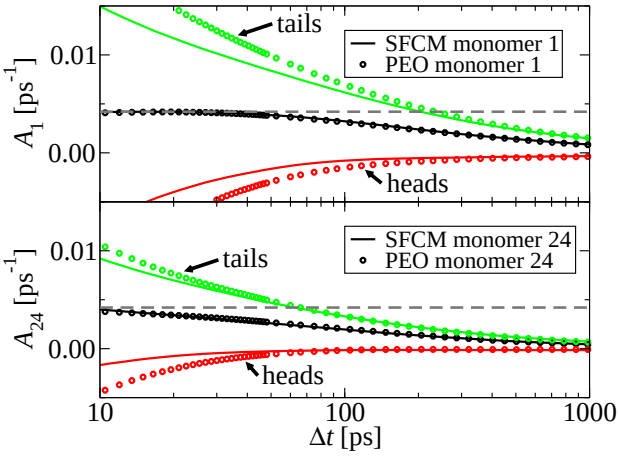

Figure 4: Effective mobilities $A_1(\Delta t)$ (top) and $A_{24}(\Delta t)$ (bottom) for the terminal and the central monomers of PEO and the SFCM. The gray dashed line indicates the plateau value of $A_n(\Delta t)$. Here, a distinction was made in which direction (relative to $\mathbf{q}_1$ or $\mathbf{q}_{24}$) the center of mass of the subchain consisting of all monomers within $\mathbf{q}_n$ moved during Δt.

ing rise to correlated motion of the chains[26]. More recently, also viscoelastic hydrodynamic interactions have been discussed[29] as a reason for the anomalous center-of-mass diffusion. Apart from this, we additionally observed in the present analysis that the center-of-mass diffusion is slightly anisotropic with respect to the orientation of the end-to-end vector $\mathbf{R}_e$ in the subdiffusive short-time regime. This is demonstrated by the inset of fig. 3, which shows the ratio of the component parallel to $\mathbf{R}_e$ relative to the total center-of-mass MSD, i. e. $\langle[(\mathbf{R}_{cm}(t+\Delta t) - \mathbf{R}_{cm}(t)) \cdot \hat{\mathbf{R}}_e(t)]^2\rangle / \langle[\mathbf{R}_{cm}(t+\Delta t) - \mathbf{R}_{cm}(t)]^2\rangle$. In the absence of anisotropies one would expect an ideal ratio of 1/3. However, the actual ratio is larger for all Δt shorter than the Rouse time ($\tau_R \approx 8.6$ ns for PEO), where the deviations increase until they reach a maximum at about 2 ns. This demonstrates that the preferential motion is along the primary axis of the chain, i. e. parallel to $\mathbf{R}_e$. In how far the observed anisotropy is related to the fact that real polymer coils are not spherical, but rather stretched in direction of $\mathbf{R}_e$[30,31] might be investigated more thoroughly in future work.

In case of the MSD of the individual monomers, one typically focuses on either the monomer-averaged MSD or, when testing the validity of specific scaling laws from e. g. the Rouse theory or the reptation model, the MSD of a few central monomers only[5–7,18], for which the characteristic features are most pronounced. For the monomeric MSDs, one generally observes that for intermediate time scales (i. e. $\tau_R/N^2 \leq \Delta t \leq \tau_R$) the outer monomers move faster than the central segments. Naturally, this regime is already highly affected by the connectivity constraints of the chain, which are less present for the end monomers. This is also confirmed in fig. 3, which shows the MSD of the terminal and the central PEO monomers in the center-of-mass frame. As stated above, the outer monomers are faster for all Δt shorter than τ_R, mainly as a result of the chain connectivity. The MSD of the respective SFCM monomers are plotted as dashed lines in fig. 3. For both the central and the outer monomers, one observes that the MSD of the SFCM is lower than the PEO curve. These deviations can be related to the more complicated local potentials for the latter system. For these reasons, it is difficult to judge whether the Rouse assumption of a uniform ζ also holds for the realistic PEO melt on the basis of the monomeric MSDs.

VI. APPLICATION OF THE PQ-METHOD

Alternatively, the local dynamics of the individual PEO monomers can be evaluated by the pq-method, yielding an effective mobility free from connectivity effects. Fig. 4 displays $A_n(\Delta t)$ for the terminal ($n = 1$, top) and the central ($n = 24$, bottom) PEO monomers. The corresponding $A_n(\Delta t)$-curves for the SFCM with a uniform ζ-value are also shown. In agreement with the Rouse model, $A_n(\Delta t)$ (i. e. the prefactor of the linear term in Eq. 2) converges to a plateau value for $\Delta t \to 0$ that is proportional to ζ_n^{-1} (indicated by the gray dashed line in fig. 4). For larger Δt, $A(\Delta t)$ decreases due to the dynamical contribution of the more remote monomers[1]. For both monomer positions, one observes a good agreement of the $A(\Delta t)$-curves of PEO (circles) and the SFCM (lines), thus demonstrating that the ζ-values of the individual PEO segments are essentially the same. As discussed previously[1], the SFCM basically captures the local dynamical features of the PEO chains in the melt already for short time scales.

In order to identify possible deviations from the rela-

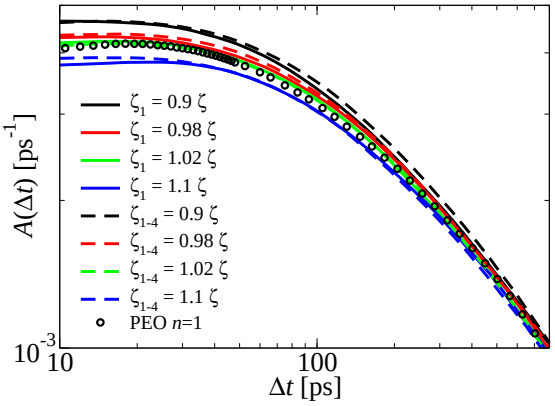

Figure 5: Effective mobilities $A_1(\Delta t)$ for the terminal monomer of a SFCM, in which (a) the terminal and (b) the four outermost monomers had a different friction coefficient (i. e. $\zeta_t = 0.9\,\zeta$, $\zeta_t = 0.98\,\zeta$, $\zeta_t = 1.02\,\zeta$) and $\zeta_t = 1.1\,\zeta$), as well as for PEO.

tion $\zeta_1 = \zeta_{24}$, we also calculated $A_1(\Delta t)$ for a SFCM, in which (a) the terminal monomer and (b) the four outermost monomers had a different friction coefficient than the other monomers (i. e. $\zeta_t = 0.9\,\zeta$, $\zeta_t = 0.98\,\zeta$, $\zeta_t = 1.02\,\zeta$) and $\zeta_t = 1.1\,\zeta$). The results are shown in fig. 5. For the extended SFCM model curves, basically two observations can be made: First, for a given ζ_t, $A_1(\Delta t)$ is nearly the same for the SFCM with ζ_t at the end monomer only and the SFCM in which the four outermost monomers have a different ζ-value. Obviously, the differences become larger if the chain ends are less mobile than the rest of the chain (i. e. for $\zeta_t = 1.1\,\zeta$). Second, from the plateau values of $A_1(\Delta t)$, one observes that the curves for which ζ_t deviates by only two percent from the ζ-values of the other monomers are clearly distinguishable. Thus, our method is able to resolve differences in the friction coefficient that are on the order of a few percent. The comparison of $A_1(\Delta t)$ of PEO with the respective SFCM curves indicates that the PEO mobility of the terminal segment is lower by about $1-2$ %. Nevertheless, one may conclude that the Rouse assumption of a constant mobility along the entire polymer chain is fulfilled for the PEO melt to a good approximation.

In principle, when only comparing the model systems, one could also obtain the same information from the short-time MSDs (not shown). However, in case of a realistic polymer chain such as PEO, exactly this regime is dominated by dynamical contributions arising from the complicated, microscopic potentials (fig. 3), and the model-chain behavior emerges only on longer time scales, for which the MSD is mainly governed by the global polymer motion. In contrast to this, our analysis is strictly local, as $A(\Delta t)$ is only sensitive to the relaxation of a given monomer within the local curvature $\mathbf{q}_n$. Accordingly, $A(\Delta t)$ remains unaltered when studying other chain lengths than $N = 48$.

Naturally, one would expect that the underlying PEO dynamics is much more complicated than that of the rather simplistic SFCM, which can already be seen from the fact that the anharmonicities are significantly larger for PEO (not shown). Therefore, we investigate the directional correlations between local chain conformation (as expressed by $\mathbf{q}_n$) and dynamics (as expressed by $\mathbf{p}_n$) in more detail, and modified our analysis in the following way: For a given displacement $\Delta\mathbf{R}_{\rm cm}^{(1-5)}(\Delta t) = \mathbf{R}_{\rm cm}^{(1-5)}(t+\Delta t) - \mathbf{R}_{\rm cm}^{(1-5)}(t)$ of the terminal Kuhn segment (monomers $1-5$, center-of-mass position $\mathbf{R}_{\rm cm}^{(1-5)}$), a distinction was made whether it moved in or against the direction of the $\mathbf{q}_1$-vector. In this way, one can distinguish between head monomers ($\Delta\mathbf{R}_{\rm cm}^{(1-5)}(\Delta t)\cdot\hat{\mathbf{q}}_1(t) > 0$), where the terminal Kuhn segment moves in front of the adjacent segments, and tail monomers ($\Delta\mathbf{R}_{\rm cm}^{(1-5)}(\Delta t)\cdot\hat{\mathbf{q}}_1(t) < 0$), where this segment follows the local chain contour. These two contributions to $A_1(\Delta t)$ are also shown in fig. 4 (upper half). The lower half of fig. 4 shows a similar head-tail analysis for monomer 24. Here, the criterion to define head and tail monomers was if the center of mass of the subchain defined by the monomers $n-\Delta n, ..., n+\Delta n$ moved in or against the direction of the $\mathbf{q}_{24}$-vector (see also sketch in fig. 1). Note that in both cases the contribution of the head monomers is partly negative, which results from their definition. Naturally, trivial head and tail contributions can also be observed for the SFCM (fig. 4) due to the bias resulting from the distinction between heads and tails. Interestingly, despite the good agreement of the average curves, the absolute values of both head and tail contributions for PEO are larger than for the SFCM. This is a consequence of the additional excluded volume, since for PEO all monomers within one Kuhn segment move much more correlated. Thus, the short-time displacement of a PEO monomer will already be dominated by the motion of the other monomers in the segment, whereas the SFCM monomers can interpenetrate each other and thus exhibit weaker motional correlations. As a result, the absolute values of $A_n(\Delta t)$ for head and tail monomers are larger for PEO. Remarkably, for both the terminal and the central monomers, the detailed interplay of intra- and intermolecular effects leads to an overall cancellation of these terms, and the local PEO dynamics in the melt is essentially the same as for a phantom chain.

VII. CONCLUSION

In this contribution, we checked the fundamental Rouse assumption of a uniform friction coefficient on all monomers for a PEO melt. The mobilities were extracted from MD simulations using our previously developed pq-method[1], which avoids the classical mode picture and rather employs a Langevin-like equation to characterize the local polymer dynamics. In contrast to the MSD, this procedure leads to the cancellation of the non-trivial terms for PEO, which arise from the additional chemical potentials. In order to interpret the local PEO dynam-

ics, we used a semiflexible phantom chain (SFCM[19]) as a reference.

During the course of our analysis it turned out that the effective mobility of both the terminal and the central PEO monomers is essentially the same as for the SFCM from about $\Delta t \geq 10$ ps on, the deviations being on the order of a few percent. However, this agreement results from the nearly quantitative cancellation of the more complicated interactions in the PEO melt. A more detailed analysis revealed that the relaxation with respect to the local chain curvature expressed by $\mathbf{q}_n$ can be decomposed in two individual contributions (i. e. head and tail monomers), depending on the direction of motion of the Kuhn segment under consideration. Due to the correlated motion in PEO arising from the excluded volume interactions, both head and tail contributions are larger for PEO. However, these contributions approximately cancel, and the mobility is roughly the same for all PEO monomers.

As reported previously[32], our findings clearly demonstrate that the pq-method yields complementary information on the dynamics of systems involving macromolecules. In further work one might study in how far the chain end effects persist or enhance when approaching the glass transition temperature (cf. the Flory-Fox equation). Moreover, the pq-method is also supposed to yield fruitful results for confined polymer melts[33,34] or complex polymer architectures[35].

Acknowledgments

The authors would like to thank Jörg Baschnagel, Hendrik Meyer and Jean Farago for helpful discussions and correspondence. Financial support from the NRW Graduate School of Chemistry is also greatly appreciated.

* Electronic address: d.diddens@uni-muenster.de

[1] D. Diddens, M. Brodeck, and A. Heuer, Europhys. Lett. **91**, 66005 (2010).
[2] P. E. Rouse, J. Chem. Phys. **21**(7), 1272 (1953).
[3] M. Doi and S. F. Edwards, *The Theory of Polymer Dynamics* (Oxford Science Publications, Clarendon, Oxford, 2003).
[4] P. G. de Gennes, *Scaling Concepts in Polymer Physics* (Cornell University Press, Ithaca, New York, 1979).
[5] K. Kremer and G. S. Grest, J. Chem. Phys. **92**(8), 5057 (1990).
[6] T. Kreer, J. Baschnagel, M. Müller, and K. Binder, Macromolecules **34**(4), 1105 (2001).
[7] W. Paul, Chem. Phys. **284**(1-2, SI), 59 (2002).
[8] M. Zamponi, M. Monkenbusch, L. Willner, A. Wischnewski, B. Farago, and D. Richter, Europhys. Lett. **72**(6), 1039 (2005).
[9] T. A. Kavassalis and J. Noolandi, Phys. Rev. Lett. **59**(23), 2674 (1987).
[10] T. A. Kavassalis and J. Noolandi, Macromolecules **21**(9), 2869 (1988).
[11] S. Rathgeber, L. Willner, D. Richter, A. Brulet, B. Farago, M. Appel, and G. Fleischer, J. Chem. Phys. **110**(20), 10171 (1999).
[12] T. G. Fox and P. J. Flory, J. Appl. Phys. **21**(6), 581 (1950).
[13] B. Schnell, H. Meyer, C. Fond, J. P. Wittmer, and J. Baschnagel, Eur. Phys. J. E **34**(9) (2011).
[14] T. Kitahara, S. Shimada, and H. Kashiwabara, Polymer **21**(11), 1299 (1980).
[15] K. A. Welp, R. P. Wool, G. Agrawal, S. K. Satija, S. Pispas, and J. Mays, Macromolecules **32**(15), 5127 (1999).
[16] Y. Miwa, K. Yamamoto, M. Sakaguchi, M. Sakai, S. Makita, and S. Shimada, Macromolecules **38**(3), 832 (2005).
[17] Y. Miwa, S. Shimada, O. Urakawa, and S. Nobukawa, Macromolecules **43**(17), 7192 (2010).
[18] W. Paul and G. Smith, Rep. Prog. Phys. **67**(7), 1117 (2004).
[19] R. Winkler, P. Reineker, and L. Harnau, J. Chem. Phys. **101**(9), 8119 (1994).
[20] A. Maitra and A. Heuer, Macromol. Chem. Phys. **208**(19-20), 2215 (2007).
[21] E. Lindahl, B. Hess, and D. van der Spoel, J. Mol. Mod. **7**, 306 (2001).
[22] O. Borodin, G. Smith, and R. Douglas, J. Phys. Chem. B **107**(28), 6824 (2003).
[23] W. Paul, K. Binder, D. W. Heermann, and K. Kremer, J. Chem. Phys. **95**(10), 7726 (1991).
[24] W. Paul, G. D. Smith, D. Y. Yoon, B. Farago, S. Rathgeber, A. Zirkel, L. Willner, and D. Richter, Phys. Rev. Lett. **80**(11), 2346 (1998).
[25] G. Smith, W. Paul, M. Monkenbusch, and D. Richter, Chem. Phys. **261**(1-2, Sp. Iss. SI), 61 (2000).
[26] J. P. Wittmer, P. Polinska, H. Meyer, J. Farago, A. Johner, J. Baschnagel, and A. Cavallo, J. Chem. Phys. **134**(23) (2011).
[27] M. Zamponi, A. Wischnewski, M. Monkenbusch, L. Willner, D. Richter, P. Falus, B. Farago, and M. G. Guenza, J. Phys. Chem. B **112**(50), 16220 (2008).
[28] M. Guenza, Phys. Rev. Lett. **88**(2), 025901 (2001).
[29] J. Farago, H. Meyer, and A. N. Semenov, Phys. Rev. Lett. **107**(17) (2011).
[30] F. Eurich and P. Maass, J. Chem. Phys. **114**(17), 7655 (2001).
[31] C. Mischler, J. Baschnagel, and K. Binder, Adv. Colloid Interface Sci. **94**(1-3, SI), 197 (2001).
[32] D. Diddens, M. Brodeck, and A. Heuer, Europhys. Lett. **95**, 56003 (2011).
[33] F. Varnik, J. Baschnagel, and K. Binder, Phys. Rev. E **65**(2, Part 1), 021507 (2002).
[34] S. Peter, H. Meyer, and J. Baschnagel, J. Polym. Sci., Part B: Polym. Phys. **44**(20), 2951 (2006).
[35] G.-L. He, H. Merlitz, J.-U. Sommer, and C.-X. Wu, Macromolecules **40**(18), 6721 (2007).

This figure "Adt_anh_head_tail.png" is available in "png" format from:

http://arxiv.org/ps/1211.3291v2

This figure "Adt_anharm_PEO_models.png" is available in "png" format from:

http://arxiv.org/ps/1211.3291v2

This figure "com_msd_inset_SFCM.png" is available in "png" format from:

http://arxiv.org/ps/1211.3291v2

This figure "ev_chain_fade.png" is available in "png" format from:

http://arxiv.org/ps/1211.3291v2

This figure "gofr1vs24_inset.png" is available in "png" format from:

http://arxiv.org/ps/1211.3291v2